machines

MDPI

Article

Comparative Study of Hydrodynamic Performance of Submerged Water Jet Propeller and Conventional Propeller Under Multiple Operating Conditions

Jiayi Li [1,2], Lei Ma [3], Dongyang Chen [1,2,4,*], Yunpeng Qi [3], Tiechao Bai [5] and Guang Pan [2]

[1] Ocean Institute, Northwestern Polytechnical University, Suzhou 215400, China; jyli@mail.nwpu.edu.cn
[2] School of Marine Science and Technology, Northwestern Polytechnical University, Xi'an 710072, China; panguang@nwpu.edu.cn
[3] Shanghai Powermaster Marine Technology Co. Ltd., Shanghai 200439, China; malei526@foxmail.com (L.M.); lechon@163.com (Y.Q.)
[4] Research Development Institute, Northwestern Polytechnical University, Shenzhen 518063, China
[5] China Ship Development and Design Center, Wuhan 430064, China
* Correspondence: cdy_1988@nwpu.edu.cn

Abstract: As global shipping accelerates toward a green and low-carbon transformation, submerged water jet propulsion has emerged as a promising alternative to traditional propellers due to its high speed efficiency, noise reduction, and adaptability. This study establishes a high-fidelity CFD (computational fluid dynamics) model incorporating vehicle body wake characteristics, validated through open-water experiments. A comparative analysis reveals that the vehicle body wake improves propulsion efficiency by 4.66% for conventional propellers and 2.32% for submerged water jet systems in near-surface operations while exacerbating cavitation-induced efficiency losses by 1.7% and 1.0%, respectively. Notably, submerged water jet propulsion demonstrates superior performance under high-velocity conditions, achieving 5–12.27% higher efficiency than conventional propellers across both open-water and vehicle body wake-affected scenarios. These findings substantiate submerged water jet propulsion's advantages in complex flow fields, offering critical insights for marine propulsion system optimization.

Keywords: submerged water jet propeller; propeller; hydrodynamic performance; cavitation performance; green ships

check for updates

Academic Editor: Zhuming Bi

Received: 26 January 2025
Revised: 10 February 2025
Accepted: 12 February 2025
Published: 13 February 2025

Citation: Li, J.; Ma, L.; Chen, D.; Qi, Y.; Bai, T.; Pan, G. Comparative Study of Hydrodynamic Performance of Submerged Water Jet Propeller and Conventional Propeller Under Multiple Operating Conditions. *Machines* **2025**, *13*, 147. https://doi.org/10.3390/machines13020147

Copyright: © 2025 by the authors. Licensee MDPI, Basel, Switzerland. This article is an open access article distributed under the terms and conditions of the Creative Commons Attribution (CC BY) license (https://creativecommons.org/licenses/by/4.0/).

1. Introduction

In the context of global climate change and environmental pollution, the marine transport industry, as one of the main forces of global trade, is facing enormous environmental pressure. As an effective means of emission reduction and energy saving, green ship design has gradually become an important direction for the development of shipbuilding industry [1]. At present, most ships use propeller propulsion. With a long history and mature technology, propeller propulsion has the advantages of simple structure, low cost, and high propulsion efficiency at low and medium speeds. However, to achieve the required propulsive efficiency at high speeds, the propeller is usually installed in the stern of the ship in an inclined way [2]. This makes the flow of the propeller uneven, leading to large flow field and thrust fluctuations and also causing significant flow-induced vibration of the stern shaft and the stern structure. The propeller excitation force can not only produce huge noise but also cause damage to the main components and mechanical equipment of the ship. In addition, under high speed conditions, the propeller blades rotate at high speed and

the tip of the blade can easily be subject to cavitation, resulting in strong cavitation noise. There are some defects in the structure form and working mechanism of propellers which make it difficult to make a big breakthrough in the propulsion and noise performance of the propeller propulsion mode after it has been improved to a certain extent [3,4].

Different from conventional propeller propulsion, submerged water jet propeller technology has a higher propulsion efficiency in a wide speed range below 40 kn, better anti-cavitation performance, and less underwater acoustic radiation [5]. The submerged water jet propeller nozzle is located underwater. The flow is more uniform and there is less pulse power. The shaft length is shortened, which makes up for the axial vibration issues. In addition, the submerged water jet propeller can maintain a high propulsion efficiency in a wide speed range, and the double shell can have a good shielding effect on underwater acoustic radiation. The application of submerged water jet propellers in medium–high-speed water surface ships can improve their propulsion efficiency and underwater noise performance, effectively reduce the fuel consumption of the ships, and increase operation comfort. In addition, submerged water jet propellers are highly integrated into the bottom of the ship, so they save space by reducing the required cabin capacity.

The research into and application of submerged water jet propellers in high-performance surface ships are mainly derived from Germany [6]. In the 1990s, the German technology company JAFO, with funding from the BMBF, developed an underwater propeller called the "LinearJet" and installed it on a flat-bottomed high-speed ship; it was tested on a model at the Potsdam Institute for Shipbuilding Testing [7]. Steden et al., at Hamburg University of Technology, optimized a linear water jet with an open-water efficiency of about 70% [8]. Due to technical limitations and other reasons, no manufacturer was able to produce such a propulsion system at that time. After entering the 21st century, the German company Voith carried out the product development of this kind of linear water jet product. It was applied to ships between 25 and 40 knots and was named Voith Linear Jet. Voith Linear Jet not only has a high propulsion efficiency in a wide speed range but also has excellent vibration and noise performance. It was successfully applied in wind field support ships in 2012 [9].

Many universities and scientific research institutions in China are also actively carrying out exploratory research on the application of submerged water jet propellers in large surface ships. For example, the Naval University of Engineering has explored the hydrodynamic characteristics of submerged water jet propellers by drawing on the technology and ideas of AWJ-21TM, an advanced electric power demonstration ship of the US Navy [10]. Cao Yuliang et al. [11,12] designed a submerged water jet propeller with reference to the AWJ-21TM water jet thruster. Based on the CFD method, the hydrodynamic performance of the submerged water jet propeller after loading was predicted, and the influence of the spray ratio on the submerged water jet thruster was studied. Peng Yunlong et al. [13] built a hydraulic design parameter selection program for submerged water jet propulsion. They used the CFD method to calculate the open water characteristics of the submerged water jet propeller and predict the propulsive performance of the submerged water jet propeller after its installation on a real-scale ship. Yi Wenbin et al. [14]. combined the ship model resistance test, ship model self-propelled test, and numerical pool simulation to analyze and explore the hydrodynamic performance of submerged water jet propellers. However, the Naval Engineering University study adopted similar design ideas and concepts as the American AWJ-21TM jet propeller, and it did not solve some of the shortcomings of the AWJ-21TM jet propeller. For example, problems such as the high resistance of the propeller pod also exist in this study. Compared with the propeller propulsion method, the propulsive efficiency advantage of the propeller is not obvious. Ding Jiangming's team at Wuhan University of Technology also continued to carry out research on high-efficiency and

low-noise submerged water jet propeller technology for several years [15,16]. In addition, there are few studies and explorations on the ship type designs suitable for submerged water jet propellers and on the factors affecting propulsion efficiency due to the lack of public reference materials and credible data support. Further studies are needed, especially on the open water and cavitation performance of submerged water jet propellers under near-surface conditions.

In this paper, the designed submerged water jet propeller and high-efficiency propeller are studied systematically, with a focus on their hydrodynamic performance and cavitation characteristics. The specific research contents are as follows: In the first and second sections, the progress of research on submerged water jet propellers in the world is described in detail, the current technical bottlenecks and future development trends are identified, and the key technical problems to be overcome in this paper are defined to provide theoretical support and research direction for subsequent research. In the third section, a high-fidelity numerical simulation model of a submerged water jet propeller is constructed based on computational fluid dynamic theory and vehicle body wake characteristics. The simulation results are compared with open water test data for the submerged water jet propeller, and the accuracy and reliability of the numerical model are quantitatively evaluated to ensure that it can accurately reflect the flow characteristics of the thrusters in the complex flow field. In the fourth section, the hydrodynamic performance and cavitation performance of the submerged water jet propeller and a conventional high-efficiency propeller under open-water conditions are compared and analyzed. The research results reveal differences in key parameters of the two thrusters, such as efficiency and thrust, under different working conditions. In order to further explore the influence of vehicle body wake on thruster performance, the submerged water jet propeller and high-efficiency propeller are coupled with a DTMB 5415 hull model [17] to simulate near-surface sailing conditions. By comparing and analyzing the hydrodynamic performance and cavitation characteristics of the two types of propellers in the wake field, the influence mechanism of vehicle body wake on the thrusters' efficiency and cavitation characteristics is quantitatively evaluated. This study provides a scientific basis for optimizing the design of propulsion systems.

2. Problem Description

In view of the shortcomings of previous studies on the open water performance and cavitation characteristics of submerged water jet propellers under near-surface conditions, this paper intends to carry out the following targeted studies:

(1) Comparative analysis of the performance of a submerged water jet propeller and a conventional propeller. The hydrodynamic performance (including thrust, efficiency, and other key parameters) of a submerged water jet propeller and a conventional high-efficiency propeller under open-water conditions and the changes in their performance after cavitation are compared. The quantitative effects of cavitation on the performance of the two thrusters are analyzed, and their advantages and limitations under different working conditions are revealed.

(2) Coupling study of propulsion performance under near-surface wake conditions. The submerged water jet propeller and high efficiency propeller are coupled with a DTMB 5415 hull model to simulate the vehicle body wake field under near-surface conditions. Based on a high-fidelity numerical simulation model, the propulsion performance of the two types of thrusters (in terms of thrust, propulsion efficiency, cavitation characteristics, etc.) in the complex wake field is deeply analyzed. The results provide a theoretical basis and technical support for the optimization of ship propulsion system design.

3. Dynamic Model and Calculation Method

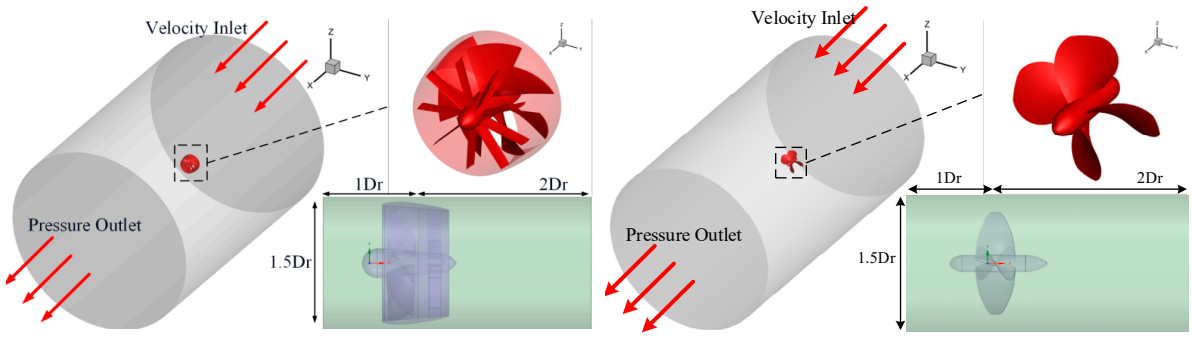
3.1. Dynamic Model

The research object of this paper is the submerged water jet propeller and high-efficiency propeller, and the inflow velocity is 18 m/s. The specific parameters of the two thrusters are shown in Table 1.

Table 1. Related parameters of conventional propeller and submerged water jet propeller.

Propeller		Submerged Water Jet Propeller	
Number of rotor blades	4	Number of rotor blades	7
Propeller diameter (mm)	1300	Rotor diameter (mm)	1333
Rotational speed (RPM)	770	Rotational speed (RPM)	535
Design hub diameter ratio	0.2	Number of stator blades	9

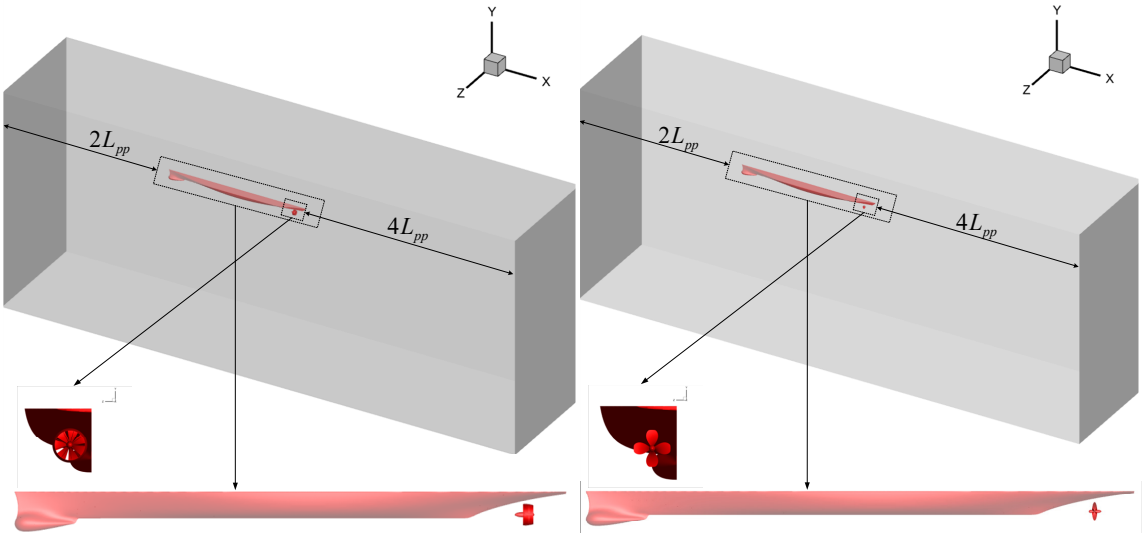
The calculation domain of the submerged water jet propeller and propeller is shown in Figure 1. The calculation domain is a cylinder with a width of 30 D_r and a length of 45 D_r, where the inlet is 15 D_r from the origin and the outlet is 30 D_r from the rotor domain. In order to better simulate the wake of the submerged water jet propeller and high-efficiency propeller, a wake encryption area is set up, which is a cylinder with a diameter of 1.5 D_r and a length of 3 D_r (where the rotor is 1 D_r from the near-field entrance). The inlet is set as the speed inlet, the outlet is set as the pressure outlet, the rotor blade and the rotor hub are set as the rotating wall, and the cylinder is set as the free slip wall.



(**a**) Submerged water jet propeller (**b**) Conventional propeller

Figure 1. Schematic diagram of calculation domain of submerged water jet propeller and conventional propeller.

The DTMB5415 ship model is used to calculate the influence of the vehicle body's wake on the performance of the submerged water jet propeller and the conventional propeller. In order to simplify the calculation [18], the part of the hull above the draught line is cut off. At the same time, half of the ship model is used for the calculation, and the calculation domain is shown in Figure 2.



(**a**) Submerged water jet propeller (**b**) Conventional propeller

Figure 2. Schematic diagram of calculation domain of submerged water jet propeller and conventional propeller considering the vehicle body's wake.

3.2. Calculation Method

(1) **Governing Equations**

In the numerical simulation, a mixed medium composed of vapor and liquid is regarded as a single fluid with variable density, and the cavitation model is introduced to describe the mass exchange between the vapor and the liquid. The continuity equation and momentum equation [19] can be expressed as

$$\frac{\partial \rho_m}{\partial t} + \frac{\partial (\rho_m u_j)}{\partial x_j} = 0 \tag{1}$$

$$\frac{\partial (\rho_m u_j)}{\partial t} + \frac{\partial (\rho_m u_i u_j)}{\partial x_j} = -\frac{\partial p}{\partial x_j} + \frac{\partial}{\partial x_j}[\mu(\frac{\partial u_i}{\partial x_j} + \frac{\partial u_j}{\partial x_j})] - \frac{\partial \tau_{ij}}{\partial x_j} \tag{2}$$

where μ is the viscosity of the fluid, ρ_m is the density of the mixed phase, and τ_{ij} is the Reynolds stress or sublattice stress tensor.

$$\rho_m = \rho_l \alpha_l + \rho_v (1 - \alpha_l) \tag{3}$$

The transport equation between the vapor and liquid is as follows:

$$\frac{\partial}{\partial x_j}(a_l u_j) + \frac{\partial (\alpha_l)}{\partial t} = (\dot{m}_c + \dot{m}_v)/\rho_l \tag{4}$$

Above, the subscript l represents the liquid phase, the subscript v represents the vapor phase, and m_c and m_v represent the vaporization rate and condensation rate, respectively, which are defined by the cavitation model adopted.

(2) **Cavitation Model**

A cavitation model is a mathematical model that describes the interaction between the gas phase and the liquid phase. Common cavitation models are described below.

(A) **Rayleigh–Plesset model**

The Rayleigh–Plesset model includes the effects of accelerated bubble growth as well as viscous effects and surface tension effects. The bubble growth rate v_r is determined using the Rayleigh–Plesset equation:

$$R\frac{dv_r}{dt} + \frac{3}{2}v_r^2 = \frac{p_{sat} - p}{p_l} - \frac{2\sigma}{\rho_l R} - 4\frac{\mu_l}{\rho_l R}v_r \tag{5}$$

where p_{sat} is the saturation pressure at a given temperature, p is the partial pressure in the surrounding liquid, σ is the surface tension, and ρ_l is the liquid density.

For multi-component cavitation, the p_{sat} term in the formula is replaced with $p_{sat,m}$, and the desired bubble growth rate can be calculated for the source term of the vapor volume fraction equation without ignoring any term in the Rayley–Plesset equation.

$$p_{sat,m} = \sum_{i}^{N_c} X_{i,l,s} p^*_{sat,i} \tag{6}$$

where $p^*_{sat,i}$ indicates the saturation pressure of the pure component, and the interface mole fraction of the liquid component is close to its volume value, so $X_{i,l,s} \approx X_{i,l}$. It should be noted that the effect of other gases present in the bubble will be ignored.

(B) **Schnerr–Sauer model** [20]

The Schnerr–Sauer cavitation model is based on the simplified Rayleigh–Plesset (RP) equation, but it ignores the effects of bubble growth acceleration, the viscosity effect, and the surface tension effect. The Schnerr–Sauer cavitation model can be used to scale the bubble growth rate and collapse rate of single-component materials and multi-component materials [21].

The cavitation bubble growth rate can be described using the inertial control growth model as follows:

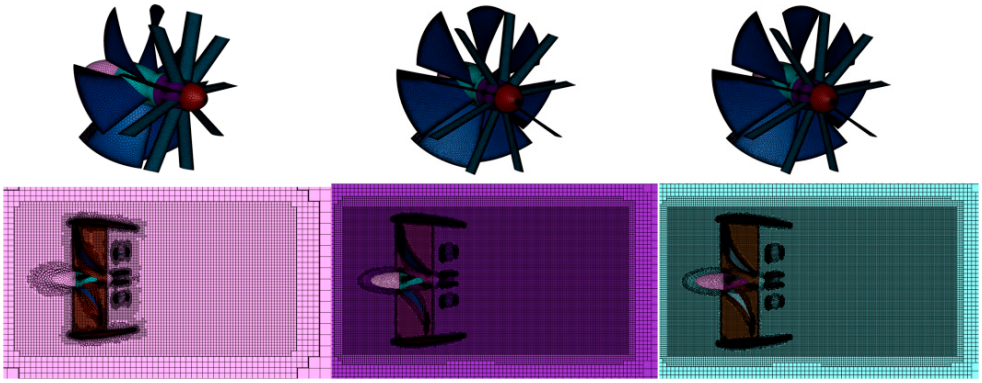
$$v_r^2 = \frac{2}{3}\left(\frac{p_{sat} - p}{\rho_l}\right) \tag{7}$$

where p_{sat} is the saturation pressure, corresponding to the temperature at the surface of the bubble, p is the pressure of the surrounding liquid, and ρ_l is the liquid density.

The Schnerr–Sauer cavitation model is a simplified form of the more general Rayleigh–Plesset (RP) equation which ignores the effects of accelerated cavity growth as well as the effects of viscosity and surface tension. Since the effects of fluid viscosity and surface tension are ignored in engineering practice, the Schnerr–Sauer cavitation model can satisfy most engineering applications. In this paper, Schnerr–Sauer cavitation model will be used for cavitation calculation.

(3) **Grid independence verification**

In order to verify the correctness of the grid division strategy, coarse, medium, and fine grids were generated according to the ITTC uncertainty analysis procedures [22]. The coarse, medium and fine grids were made to ensure that Y^+ was basically consistent among the different grids and in line with the requirements of turbulence model for near-wall grids. The three sets of grid diagrams are shown in Figure 3 and Table 2.



(**a**) (**b**) (**c**)

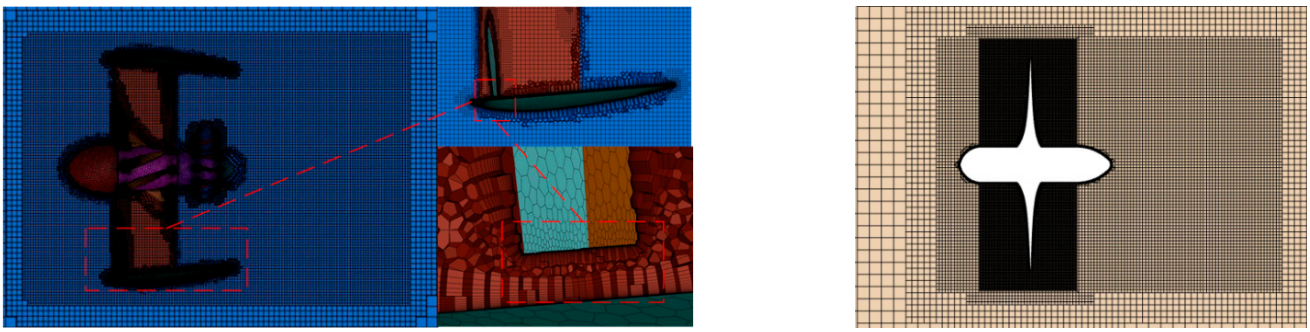
Figure 3. Schematic diagrams of three grids: (**a**) coarse grids, (**b**) medium grids, and (**c**) fine grids.

Table 2. Calculation results of three kinds of grids.

Mesh	Total Number of Grids	K_{Tr}	Error/%	10 K_{Qr}	Error/%
Coarse	8.53 Million	0.5521	6.81%	1.5983	−1.64%
Medium	13.94 Million	0.5661	4.44%	1.5925	−1.30%
Fine	22.10 Million	0.5693	3.91%	1.5892	−1.07%

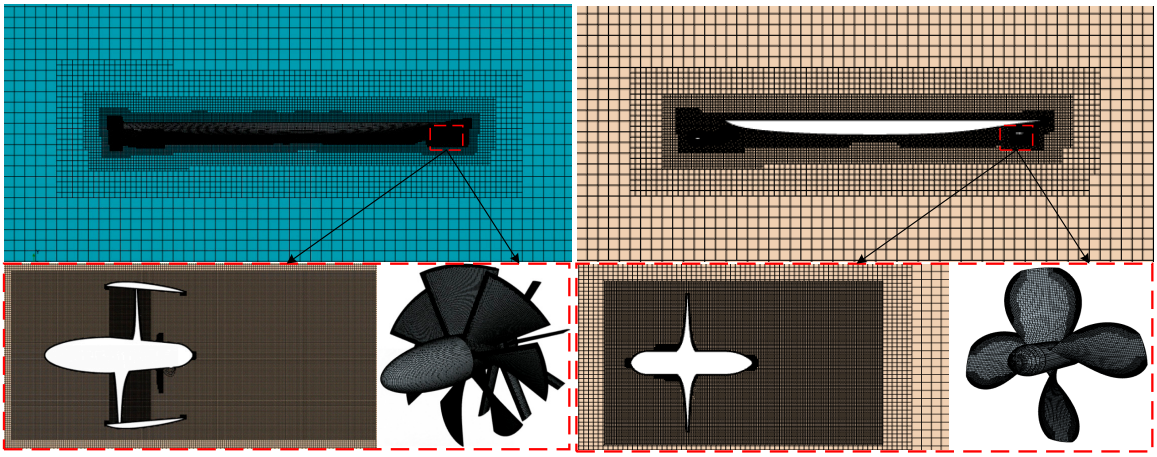
It can be seen that the calculation results of K_{Tr} and 10 K_{Qr} of the submerged water jet propeller using medium grids and fine grids have less error compared with the reference value, while the calculation results of coarse grids have a big difference compared to the other two grids, and the subsequent calculations will be carried out using medium grids in consideration of the calculation time.

According to the above medium grid division method, the submerged water jet propeller, conventional propeller, and DTMB5415 ship are meshed. The grid details are shown in Figures 4 and 5. The total number of grids for the propeller is about 6.121 million, the total number of grids for the submerged water jet propeller is about 13.94 million, the total number of grids for the whole ship coupled with the propeller is about 14.221 million, and the total number of grids for the whole ship coupled with the submerged water jet propeller is about 14.121 million.



(**a**) Submerged water jet propeller (**b**) Conventional propeller

Figure 4. Schematic diagram of propeller grids and submerged water jet propeller grids.



(**a**) Submerged water jet propeller (**b**) Conventional propeller

Figure 5. Schematic of the grids of the hull coupled with the conventional propeller and the grids of the hull coupled with submerged water jet propeller.

3.3. Dynamic Model and Calculation Method Verification

3.3.1. Validation of Open-Water Performance Simulation Method

The submerged water jet propeller flow field test is an important means to verify the accuracy of the numerical simulation of the thruster flow field conducted in this paper. The open-water performance test experiment of the submerged water jet propeller was carried out in the cavitation tunnel of Shanghai Ship Transportation Science Research Institute Co., Shanghai, China. The main technical parameters of the cavitation tunnel are as follows: length: 26.9 m, height: 50.0 m. The main parameters of the working section are as follows: diameter: 0.8 m, length: 3.2 m; water velocity: 1.0 m/s~20.0 m/s; pressure range: 8 kPa~400 kPa. The working section of the water cylinder as well as the assembly of the model are shown in Figure 6.

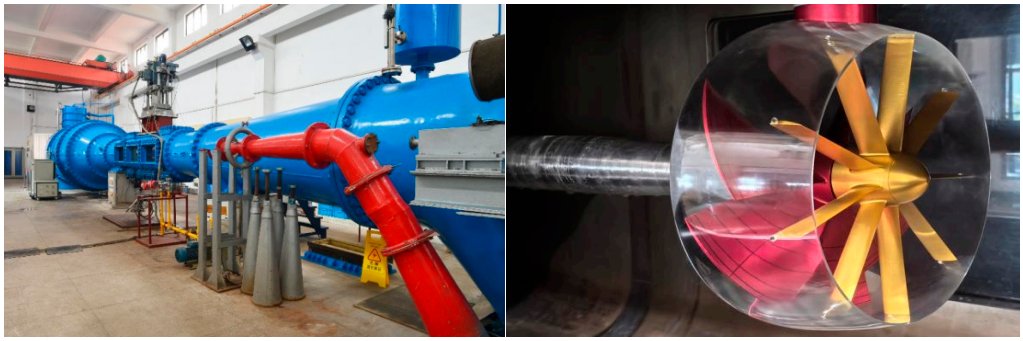


Figure 6. Working section of the cavitation tunnel and schematic diagram of the model.

In the experimental test, the stator and the duct are fixedly connected by screws, so the force or moment of the stator and the duct cannot be distinguished. N is the rotor speed (r/s), V is the far-field incoming velocity (m/s), D is the diameter of the rotor blade, and ρ is the density of fluid (kg/m^3). Under the experimental conditions, the rotational speed of the rotor is 960 RPM, and the advance ratio J is adjusted by changing the incoming velocity. The experimental test range of J is 0.35–1.92.

The error comparison with the experimental data is shown in Figure 7 below.

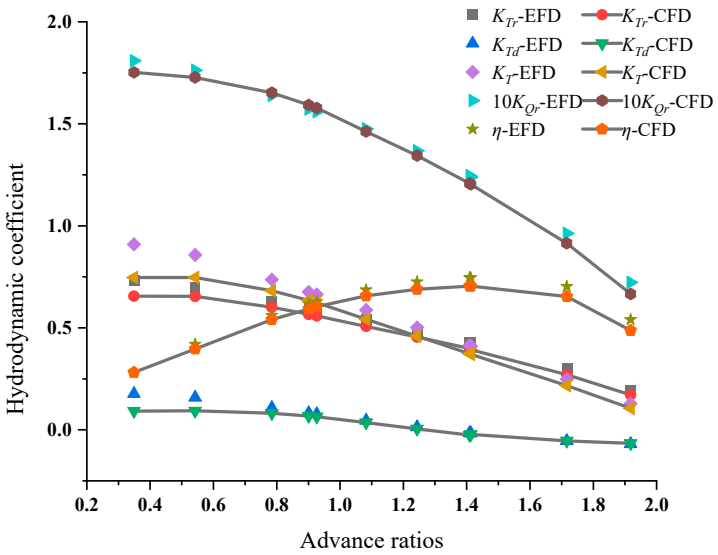


Figure 7. Hydrodynamic coefficient simulation results of the submerged water jet propeller compared with experimental data.

Overall, the comparison between the numerical simulation results and the experimental data shows a high degree of agreement, and the error is within a reasonable range. Under the open-water condition, the largest error occurs when the advance ratio is 1.7, with an error of 7%; the smallest error occurs when the advance ratio is 0.35, with an error of only 1%. Considering that the experimental model inevitably has machining errors during the machining process, especially in the rotor and stator roots, due to the limitation of the machining process, the experimental model has rounded root corners, which is a geometrical feature that is not taken into account in the numerical simulation. In addition, in the actual experimental process, limited by the installation conditions, a certain installation deviation will inevitably occur. All these factors will have some influence on the comparison between the experimental results and the numerical simulation results. Therefore, the above errors are within the acceptable range and can meet the requirements of the experimental study, thus verifying the accuracy and reliability of the numerical calculation method adopted in this paper.

3.3.2. Validation of Cavitation Performance Calculation Method

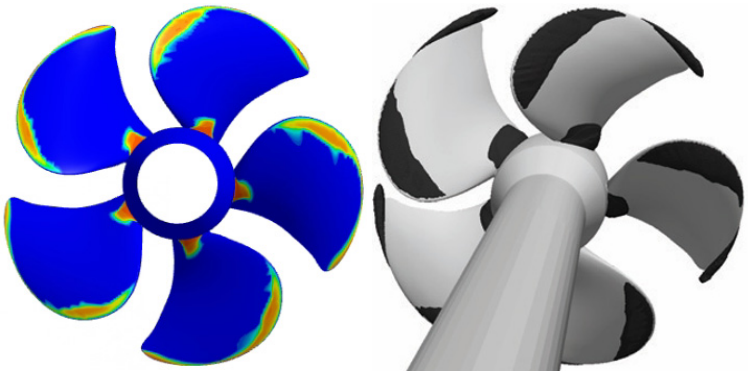
This paper takes the PPTC propeller [23] commonly used in the calculation of cavitation as an example to verify the calculation method, and its specific parameters are shown in Table 3. The same mesh topology is used to generate three sets of unstructured meshes with increasing mesh numbers. Calculations are carried out under the working conditions of rotational speed n = 24.987 r/s, advance ratio J = 1.019, and cavitation number σv = 2.024 [24]. Based on the above three sets of grids, the PPTC propeller was numerically simulated, and the thrust coefficient was calculated and compared with the experimental results. The comparison results are shown in Table 4, and the comparison of cavitation contour is shown in Figure 8. It can be seen that the three sets of grids simulation results are very close to the test results, and the difference between the calculation results of medium grids and fine grids is small, so the rationality of the mesh division strategy and of the calculation method is verified.

Table 3. PPTC propeller parameters.

	PPTC	
Diameter (m)	D	0.250
Hub diameter ratio	d/D	0.300
Pitch ratio	$P_{0.7}/D$	1.635
Blade area ratio	A_e/A_o	0.779
Number of blades	Z	5

Table 4. Comparison of thrust coefficients before and after cavitation with experimental data.

Grid Type	Total Number of Grids	K_T		
		CFD	**EFD**	**Error/%**
Coarse	1.13 Million	0.3490	0.3870	9.8%
Medium	3.56 Million	0.3655	0.3870	5.5%
Fine	6.32 Million	0.3753	0.3870	3.02%
		K_T (Cavitation)		
		CFD	EFD	Error/%
Coarse	1.13 Million	0.342	0.3725	8.0%
Medium	3.56 Million	0.353	0.3725	5.2%
Fine	6.32 Million	0.358	0.3725	3.89%



(**a**) (**b**)

Figure 8. Contour of PPTC propeller cavitation. (**a**) CFD contour. (**b**) EFD contour [25].

4. Analysis of Calculation Results

4.1. Analysis of Open-Water Performance of Submerged Jet Propeller and Conventional Propeller

Firstly, the open-water performance of the submerged water jet propeller and the conventional propeller was calculated and compared [26]. The performance curve of the full advance ratios of the submerged water jet propeller was calculated, and the calculation results are shown in Table 5 and Figure 9.

Table 5. Results of open-water performance for full advance ratios of submerged water jet propeller.

Velocity (m/s)	Advance Ratios	Thrust (10^4 N)	Power (MW)	Efficiency	RPM
4	0.337	21.372	3.448	0.2479	535
6	0.505	21.112	3.400	0.3705	535
8	0.673	17.219	2.856	0.4761	535
10	0.841	15.551	2.718	0.5721	535
12	1.010	14.192	2.625	0.6485	535

Table 5. *Cont.*

Velocity (m/s)	Advance Ratios	Thrust (10^4 N)	Power (MW)	Efficiency	RPM
14	1.178	12.921	2.572	0.7032	535
16	1.346	11.531	2.490	0.7407	535
18	1.514	9.068	2.154	0.7575	535
20	1.683	6.847	1.834	0.7463	535
22	1.851	4.564	1.463	0.6864	535

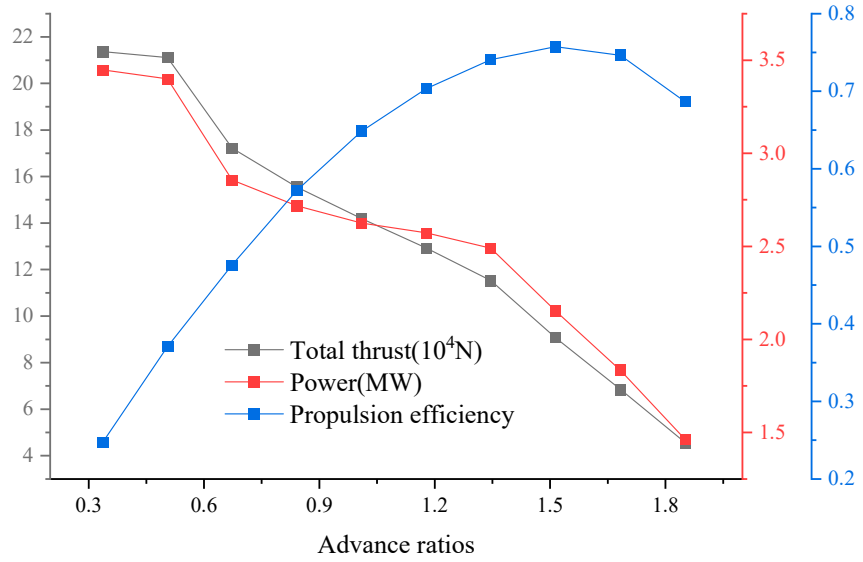


Figure 9. Comparison curves of open water efficiency, power, and total thrust of submerged jet propellers.

Since the thrust and torque of the conventional propeller are very large at low speeds, there is no reference for comparison with the performance of the submerged water jet propeller, so only the designed working condition of the propeller is calculated, that is, an inflow velocity is 18 m/s. The hydrodynamic performance of the propeller under this working condition is shown in Table 6.

Table 6. Hydrodynamic performance of propeller under 18 m/s condition.

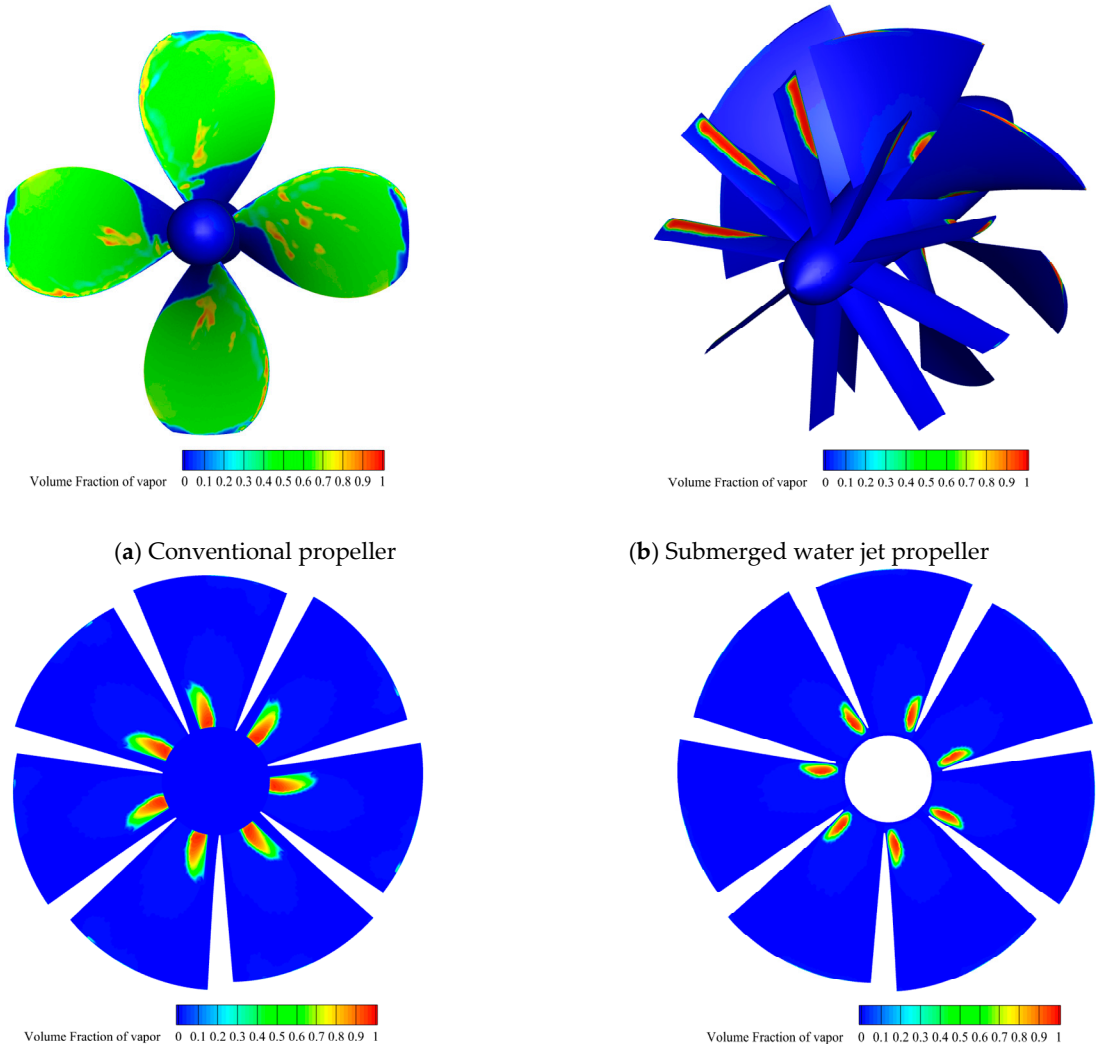
Rotational Speed	Inflow Velocity (m/s)	Efficiency	Thrust (10^4 N)
770 RPM	18	0.6908	9.356

From the above table and curve analysis, it can be seen that the peak open-water efficiency of the submerged water jet propeller is 6.67% higher than that of the conventional propeller. This performance advantage is mainly attributed to the special layout of the submerged water jet propeller, where the stator is located downstream of the rotor. This layout effectively recovers the rotational kinetic energy in the rotor wake stream, significantly reducing energy dissipation. Through this energy recovery mechanism, the thruster achieves higher propulsive efficiency over a wide range of advance ratios, especially at high speeds. This characteristic suggests that the submerged water jet propeller has significant efficiency advantages under high speed conditions and can provide more efficient power support for ships.

4.2. Cavitation Performance Analysis of Submerged Water Jet Propeller and Conventional Propeller

The cavitation performance of the submerged water jet propeller and the conventional propeller is analyzed below. The cavitation model adopts the Schnerr–Sauer cavitation

model. Since the working conditions studied in this paper are actual ship operating conditions, there is no fixed cavitation number, and the environmental pressure of the propeller can only be specified as the pressure at 3 m underwater. The saturated vapor pressure is 3170 Pa. The cavitation contour and calculation results for the conventional propeller and the submerged water jet propeller are shown in Figures 10 and 11 and Table 7.



(**a**) Conventional propeller (**b**) Submerged water jet propeller

(**c**) Rotor suction surface (**d**) Rotor pressure surface

Figure 10. Cavitation contours of submerged water jet propeller and conventional propeller.

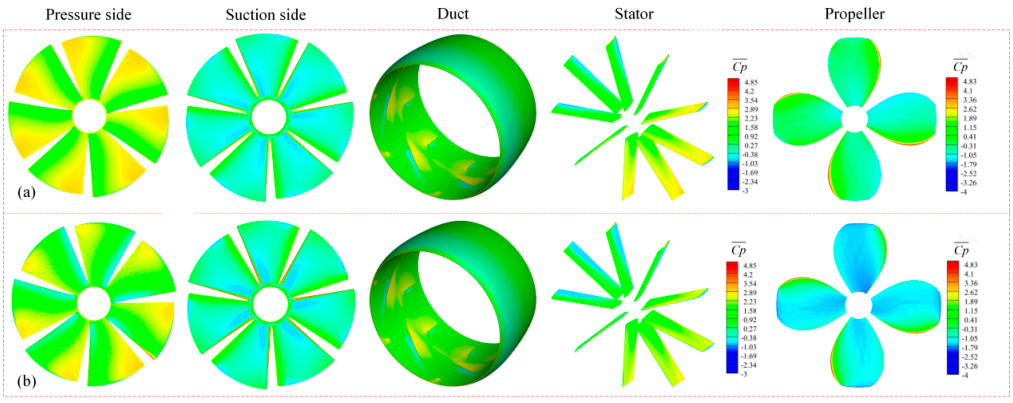


Figure 11. Pressure coefficient contours of various components of the submerged water jet propeller and conventional propeller before and after cavitation: (**a**) before cavitation, (**b**) after cavitation.

Table 7. Hydrodynamic performance table of propeller and submerged water jet propeller before and after cavitation.

	Inflow Velocity (m/s)	Efficiency	Efficiency (Cavitation)	Thrust (10^4 N)	Thrust (Cavitation) (10^4 N)
Propeller	18	0.6908	0.631	9.356	7.149
Submerged water jet propeller	18	0.7575	0.7507	9.068	9.018

From the pressure coefficient contours, it can be seen that after the fluid begins to enter the rotor domain, the fluid in the rotor domain is accelerated by the rotating acceleration of the rotor. The pressure near the blade tip of the rotor pressure surface is large, which promotes the development of the fluid. The highest-pressure point of the rotor appears at the leading edge of the pressure surface, while the pressure level of the rotor suction surface is low. In particular, there is a relatively obvious low-pressure area near the tip of the leading edge, which is mainly caused by the tip leakage vortex generated by the clearance flow. In addition, there are also obvious low-pressure areas near the rotor hub and in front of the rotor at the tail of the stator. As can be seen from the cavitation contour, these areas are also prone to the cavitation phenomenon. The pressure distribution on the outer wall of the duct is more uniform, and there is a more obvious pressure gradient at the front of the duct, and the pressure at the front of the duct is larger. This is mainly due to the impact of incoming flow. It can also be seen from the contour that the pressure distribution law of the pressure surface and suction surface of the stator blade is basically the same as that of the rotor blade. This is mainly because the distance between the rotor and the stator is small, and the flow field in the stator domain is greatly affected by the flow field in the rotor domain, and the pressure characteristics of the flow field in the rotor domain are basically maintained. However, because the stator has an obvious reverse velocity gradient, and because the stator can convert a part of the tangential velocity into axial velocity by performing work on the fluid, thus generating a small amount of extra thrust, the change in the pressure distribution of the stator blade is not as obvious as that of the rotor blade.

From the analysis of the cavitation contour, it can be seen that the tip of the propeller blade has a large linear velocity, and the local pressure can easily fall below the saturated vapor pressure, which triggers a significant cavitation phenomenon. The cavitation area is widely distributed in the whole rotor surface, showing different degrees of flaky cavitation and cloudy cavitation. At this time, the rotational speed of the propeller is 770 RPM, and the advance ratio is 1.08, which is close to an advance ratio of 1.258, corresponding to the highest efficiency point of the real-scale model. According to the performance characteristics of the propeller, the optimal efficiency point is usually taken to be about 70% of the advance ratio corresponding to the highest efficiency point, and after exceeding this value, the propeller's thrust and efficiency will be drastically reduced. Therefore, under this high-risk condition, even if 18 m/s and 770 RPM are selected as the optimal efficiency point of the propeller, its open-water efficiency is only 69.08%, and the efficiency is further reduced to 63.1% after cavitation.

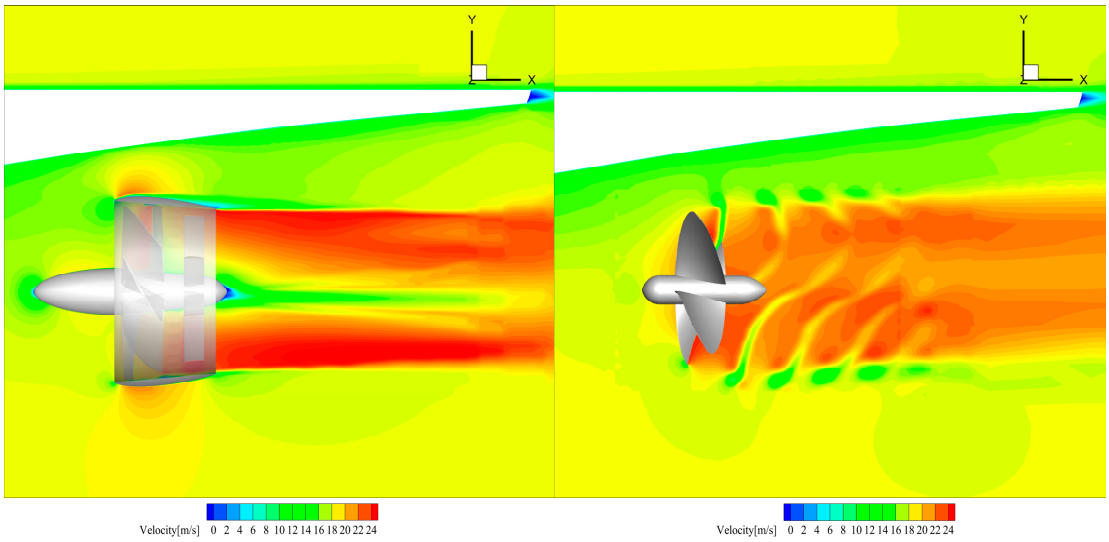
In contrast, the cavitation area of the submerged water jet propeller is mainly concentrated in the rotor suction surface near the leading edge and the blade top area. At the same time, due to the influence of the inlet angle, local cavitation also occurs in the rotor pressure surface near the hub. The stator can effectively rectify the rotational energy in the rotor wake and convert circumferential motion into axial motion. This improves the contraction phenomenon of the hub wake, avoids the unnecessary consumption of energy here, eliminates the low-pressure area in the wake, and significantly reduces the cavitation effect. This design enables the submerged water jet propeller to maintain high propulsive

efficiency under cavitation conditions, especially at high speeds, where the performance advantage is more significant.

In summary, the performance of the submerged water jet propeller at high speeds is significantly better than that of the conventional high-efficiency propeller, especially in terms of its ability to maintain efficiency under cavitation conditions, which is a significant advantage for engineering applications.

4.3. Performance Analysis of Submerged Water Jet Propeller and Conventional High-Efficiency Propeller Considering the Influence of Vehicle Body Wake

In the previous section, the open-water performance and cavitation performance of the submerged water jet propeller and the conventional high-efficiency propeller were calculated, and it was found that the performance of the submerged water jet propeller was significantly better than that of the conventional propeller. In this section, the performance of the submerged water jet propeller and the conventional high-efficiency propeller is calculated and compared while taking the influence of the vehicle body's wake into consideration. The calculation results are shown in Figure 12 below.

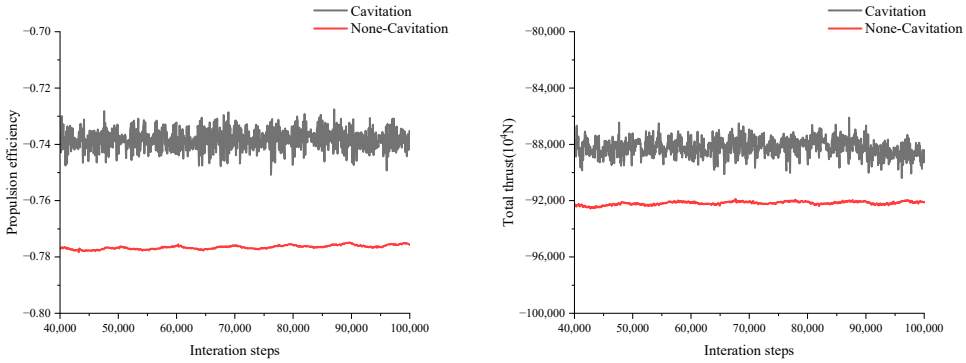


(**a**) Submerged water jet propeller (**b**) Conventional propeller

Figure 12. Velocity contour of submerged water jet propeller and conventional high-efficiency propeller flow field in X-Y section.

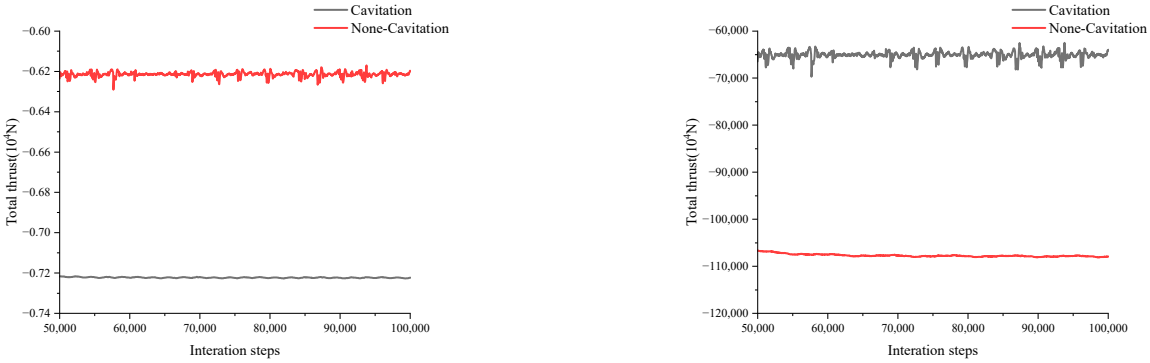
As can be seen from the velocity contour of the submerged water jet propeller, the velocity of its external flow field basically presents a linear distribution, and the flow field structure is relatively clear and simple, belonging to the outflow problem in a large space. The flow field in the duct has a direct effect on the outflow field, and it can be seen from the contour that the wake acceleration brought by the duct is obvious. The value of wake axial velocity is much larger and more uniform, resulting in an obvious propulsion effect.

It can be seen from the curves in Figures 13 and 14, considering the influence of the vehicle body's wake, the total thrust of the propeller before cavitation is about 10.8×10^4 N, and the total thrust after cavitation is about 6.5×10^4 N under the condition that the incoming flow velocity is 18 m/s. The propulsion efficiency of the propeller before cavitation is about 72.3%, and after cavitation, it is about 62%. The total thrust of the submerged water jet propeller before cavitation is about 9.22×10^4 N, and after cavitation, it is about 8.7×10^4 N. The propulsive efficiency of the submerged water jet propeller is about 77.5% before cavitation and 74.27% after cavitation.



(**a**) Propulsion efficiency (**b**) Total thrust

Figure 13. Performance curves of submerged water jet propeller considering effect of vehicle body wake.

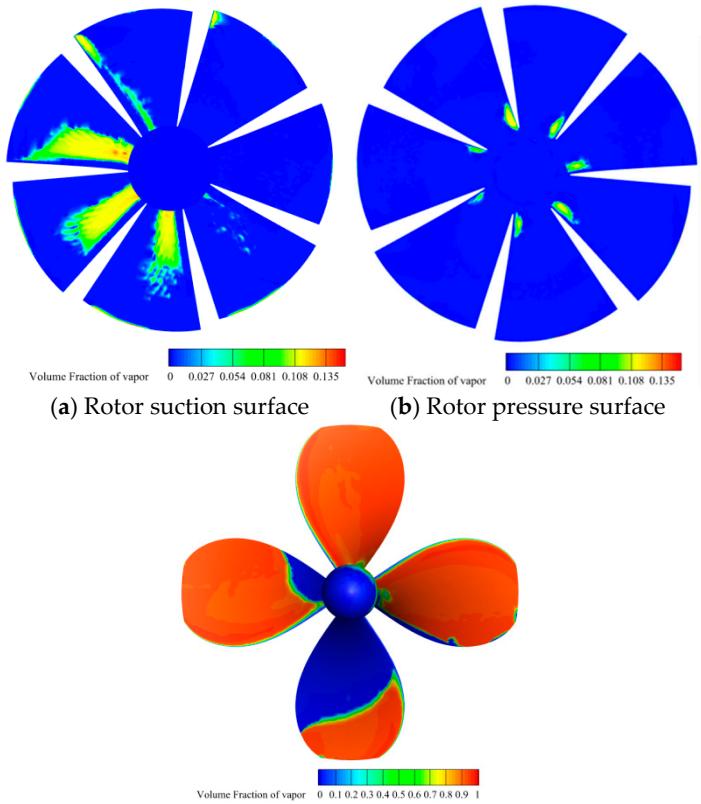


(**a**) Propulsion efficiency (**b**) Total thrust

Figure 14. Performance curves of propeller considering effect of vehicle body wake.

From the above curves, it can also be found that the total thrust and propulsive efficiency curves before cavitation are relatively smooth, while those after cavitation show fluctuations of different magnitudes. This is because when the cavitation phenomenon occurs, the local pressure on the surface of the blade decreases below the saturated vapor pressure, forming bubbles. The existence of these bubbles changes the pressure distribution on the blade surface. Moreover, the collapse of these bubbles will produce local high-pressure shock waves and micro-jets, strip the surface of the blade, and at the same time cause intense pulsating pressure. This pulsating pressure not only reduces the thrust of the blade but also leads to an increase in the vibration and noise of the blade. In addition, the high-pressure shock wave generated in the process of vacuole collapse will make the pressure distribution on the blade surface more complicated, which further affects the stability of the thrust and propulsion efficiency. And the cavitation phenomenon will lead to a constant change in the cavitation region on the blade surface, which may expand or shrink rapidly. This instability makes it difficult to keep the pressure distribution and thrust output of the blade stable, leading to drastic fluctuations in thrust and efficiency.

The three contours in Figure 15 are are the cavitation contours of the conventional propeller and the submerged water jet propeller considering the influence of the vehicle body's wake. It can be seen that under the condition of an inflow velocity of 18 m/s, a large cavitation area occurs on the whole rotor surface of the propeller, and the hydrodynamic performance also deteriorates significantly. For the submerged water jet propeller, cavitation mainly occurs at the leading edge of the rotor suction surface, and a small cavitation area also occurs at the pressure surface near the leading edge and the hub due to the influence of flow angle.



(**a**) Rotor suction surface (**b**) Rotor pressure surface

(**c**) Propeller rotor

Figure 15. Cavitation contours of propeller and submerged water jet propeller considering effect of vehicle body wake.

As can be seen from the pressure coefficient contours in Figure 16, considering the role of the vehicle body's wake, the pressure distribution of each component of the submerged water jet propeller and conventional propeller is basically the same as that under the open-water condition described in the previous section. However, the vehicle body wake causes the low-pressure area on the rotor and stator of the submerged water jet propeller and on the rotor of the conventional propeller, which is prone to cavitation, to gradually expand. That is, the vehicle body's wake will aggravate the cavitation of the submerged water jet propeller and conventional propeller.

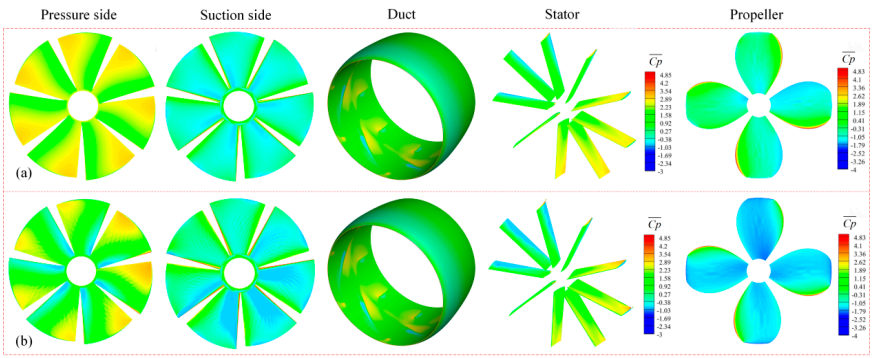


Figure 16. Pressure coefficient contours of various components of the submerged water jet propeller considering the effect of the vehicle body's wake before and after cavitation: (**a**) before cavitation, (**b**) after cavitation.

In order to make a more convenient comparison, the calculation results of the conventional propeller and the submerged water jet propeller in this section are summarized under different working conditions, and the results are shown in Table 8.

Table 8. Summary of hydrodynamic performance of submerged water jet propeller and conventional propeller under different working conditions.

Working Conditions	Inflow Velocity (m/s)	Propulsion Efficiency	Thrust (10^4 N)	Thrusters
Coupled with DTMB5415	18	0.775	9.22	Submerged water jet propeller
Coupled with DTMB5415	18	0.723	10.8	Propeller
Coupled with DTMB5415 (Cavitation)	18	0.7427	8.7	Submerged water jet propeller
Coupled with DTMB5415 (Cavitation)	18	0.62	6.5	Propeller
Open water	18	0.7575	9.068	Submerged water jet propeller
Open water	18	0.6908	9.356	Propeller
Open water (Cavitation)	18	0.7507	9.018	Submerged water jet propeller
Open water (Cavitation)	18	0.631	7.149	Propeller

It can be seen that the effect of vehicle body wake flow causes an increase in the total thrust of the submerged water jet propeller and the conventional propeller, resulting in a further increase in propulsive efficiency. The reason is that the flow field formed in the wake of the ship while sailing is non-uniform, and its velocity distribution and pressure distribution are different from those of the surrounding flow field. The presence of the wake flow increases the inlet velocity of the thruster, especially near the thruster disk, and the increase in flow velocity helps to increase the thrust and efficiency of the thruster. Moreover, the wake contains part of the energy generated by the ship, which can be recovered and converted into thrust when the thruster works in the wake. This energy recovery mechanism makes the efficiency of the thruster under actual working conditions higher than that under open-water conditions alone. However, the vehicle body's wake also further exacerbates the total thrust and propulsive efficiency losses of the submerged water jet propeller and conventional propeller after cavitation due to the fact that the vehicle body's wake is non-uniform, with velocity and pressure distributions that differ significantly from those of a uniform flow field. This non-uniformity alters the inlet flow conditions of the propeller, causing the pressure in localized regions to decrease more rapidly, thus exacerbating cavitation. Under low-advance-ratio conditions, the low-velocity region in the wake flow may cause the local pressure to decrease to the vaporization pressure, which triggers cavitation in advance. Moreover, the presence of the vehicle body's wake flow will expand the cavitation region; especially, the cavitation initialization in the region at the back of the blade is advanced, and the cavitation range is increased significantly. The expansion of the cavitation region leads directly to a reduction in the effective working area of the propeller, which in turn reduces the thrust output.

As can be seen from the data in the table, the submerged water jet propeller significantly outperforms the conventional high-efficiency propeller in terms of its hydrodynamic performance and cavitation characteristics, both in open-water conditions and in conditions that take into account the vehicle body wake effects. The propulsive efficiency of the submerged water jet propeller is at least 5% and up to 12.27% higher than that of the conventional high-efficiency propeller in all conditions. This indicates that under high-speed conditions near the water surface, the submerged water jet propeller can effectively improve the propulsion efficiency and reduce the risk of cavitation by its unique energy recovery mechanism and its ability to inhibit the cavitation phenomenon, which makes it an ideal choice for the propulsion system of high-speed ships.

5. Conclusions

In this paper, the hydrodynamic performance and cavitation performance of the designed submerged water jet propeller and high-efficiency propeller are calculated under open-water conditions. In addition, the hydrodynamic performance and cavitation performance of the submerged water jet propeller and conventional high-efficiency propeller under vehicle body wake are also calculated by matching them with the DTMB5415 ship model, and the results are compared and summarized, and the following conclusions are drawn:

1. The submerged water jet propeller can still maintain high propulsive efficiency at high speeds, with a peak propulsive efficiency of 75.75%, while the propulsive efficiency of the conventional high-efficiency propeller decreases significantly at high speeds, and at the same speeds, the propulsive efficiency of the submerged water jet propeller is 6.77% higher than that of the propeller. In the near-surface environment, even if cavitation occurs, the performance of the submerged water jet propeller is obviously superior to that of the high efficiency propeller.
2. The wake flow of the vehicle body wake can significantly improve the propulsive efficiency of the submerged water jet propeller and the conventional propeller, and the propulsive efficiencies of the conventional propeller and the submerged water jet propeller are improved by 4.66% and 2.32%, respectively. At the same time, the vehicle body wake will also exacerbate the reduction in propulsion efficiency after cavitation occurs, and the propulsion efficiencies of the propeller and the submerged water jet propeller are reduced by 1.7% and 1.0%, respectively.
3. In near-surface environments, the performance of submerged water jet propellers is significantly better than that of high-efficiency propellers when the effect of the vehicle body's wake is considered. The propulsion efficiency of submerged water jet propellers is at least 5% and up to 12.27% higher than that of conventional high-efficiency propellers. Therefore, submerged water jet propellers have a broad application prospect when they are applied to high-speed surface vessels.

Author Contributions: J.L.: investigation (lead); software (equal); writing—original draft (lead). L.M.: investigation (equal); validation (equal). D.C.: conceptualization (equal); writing—review and editing (lead). Y.Q.: investigation (equal); validation (equal). T.B.: investigation (equal); validation (equal). G.P.: conceptualization (equal). All authors have read and agreed to the published version of the manuscript.

Funding: This research work is supported by the National Natural Science Foundation of China (No. 52471342), the Guangdong Basic and Applied Basic Research Foundation (No. 2024A1515011046), the China Postdoctoral Science Foundation (No. 2023M743108), the Zhejiang Province Leading Innovation and Entrepreneurship Team Project (No. 2022R01012), and the Gusu Youth Innovation Leading Talent Project (No. ZXL2023168). The authors would like to dedicate this work to the late Professor Laith K. Abbas of Nanjing University of Science and Technology, Nanjing (NJUST).

Data Availability Statement: Data available on request from the authors.

Conflicts of Interest: Authors Lei Ma and Yunpeng Qi were employed by the company Shanghai Powermaster Marine Technology Co., Ltd. The remaining authors declare that the research was conducted in the absence of any commercial or financial relationships that could be construed as a potential conflict of interest.

References

1. Zou, S.J.; Kong, F.P. Research on green ship design and sustainable development. *Ship Mater. Mark.* **2024**, *32*, 81–83.
2. Wang, H.Q. *Research on Submerged Water Jet Propulsion Scheme for Drainage Type Medium and High Speed Vessels*; Wuhan University of Technology: Wuhan, China, 2021.

3. Li, C.; Hao, W.; Lei, W.; Liu, M.; Hua, H. Vibro-acoustic responses of a hull due to structural and acoustic excitations from a propeller. *Ocean Eng.* **2023**, *276*, 114–168. [CrossRef]
4. Posa, A.; Broglia, R.; Balaras, E.; Felli, M. The acoustic signature of a propeller–hydrofoil system in the far field. *Phys Fluids* **2023**, *7*, 75–101. [CrossRef]
5. Ding, J.M.; Wang, Y.S.; Liu, C.J. Analysis on the application of water jet propulsion in modern ships. *Ship Sci. Technol.* **2006**, *28*, 28–31.
6. Ding, J.M. Current status of domestic and international research and application of water jet propulsion technology for ships. In Proceedings of the 2013 Ship Hydrodynamics Conference, Xi'an, China, 13–15 August 2013.
7. Bohm, M.; Jurgens, D. Linear-Jet: A Propulsion System for Fast Ships. In Proceedings of the 7th International Symposium on Practical Design of Ships and Mobile Units, Hague, The Netherlands, 20–25 September 1998.
8. Steden, M.; Hundemer, J.; Moustafa, A. Optimisation of a linear jet. In Proceedings of the First International Symposium on Marine Propulsors, Trondheim, Norway, 22–24 June 2009.
9. Wang, L.X. *Water Jet Propulsion Technology and Engineering Design*; National Defense Industry Press: Beijing, China, 2021; pp. 180–181.
10. Giles, W.; Dinham-Peren, T.; Amaratunga, S.; Vrijdag, A.; Partridge, R. The Advanced Waterjet: Propulsor Performance and Effect on Ship Design. In Proceedings of the IMAREST's 10th International Naval Engineering Conference, Portsmouth, UK, 11–13 May 2010; [s.l.]: Rolls Royce Plc, BMT Defence Services Ltd.: Bath, UK, 2010.
11. Cao, Y.L.; Wang, Y.S.; Jin, B.B. Design of submerged water jet propulsion pump and performance prediction after ship loading. *J. Xi'an Jiaotong Univ.* **2014**, *48*, 96–101.
12. Cao, Y.L.; Wang, Y.S.; Yi, W.B.; Jin, S. Effect of jet speed ratio on the propulsive performance of submerged water jet propellers. *J. Harbin Eng. Univ.* **2015**, *36*, 894–898.
13. Peng, Y.L.; Wang, Y.S.; Cao, Y.L. Design parameter selection and performance analysis of real-scale submerged water jet propulsion pump. *J. Ship Mech.* **2016**, *20*, 947–953.
14. Yi, W.B.; Wang, Y.S.; Liu, C.J.; Peng, Y.L. Self-propulsion test and numerical simulation of submerged water jet propulsion. *Ship Mech.* **2017**, *21*, 407–412.
15. Fu, J.; Ding, J.M.; Li, J. Numerical prediction of hydrodynamic noise of submerged water jet propeller. *J. Dalian Marit. Univ.* **2023**, *49*, 85–92.
16. Fu, J.; Ding, J.M.; Xie, Y. Numerical analysis of pulsating flow field characteristics of submerged water jet propeller. *Mar. Eng.* **2024**, *53*, 6–10.
17. Olivieri, A.; Pistani, F.; Avanzini, A.; Stern, F.; Penna, R. *Towing Tank Experiments of Resistance, Sinkage and Trim, Boundary Layer, Wake, and Free Surface Flow Around a Naval Combatant INSEAN 2340 Model*; The University of Iowa: Iowa City, IA, USA, 2001.
18. Ma, J.; Lai, M.Y.; Wei, B. Numerical analysis of aft propeller hydrodynamics in oblique flow. *Ship Eng.* **2019**, *41*, 31–36.
19. Ferziger, J.H.; Peric, M. *Computational Methods for Fluid Dynamics*, 3rd ed.; Springer: Berlin, Germany, 2002; 426p.
20. Schnerr, G.H.; Sauer, J. Physical and Numerical Modeling of Unsteady Cavitation Dynamics. In Proceedings of the 4th International Conference on Multi-Phase Flow, New Orleans, LA, USA, 27 May–1 June 2001.
21. Liu, D. The numerical simulation of propeller sheet cavitation with a new cavitation model. *Proceedia Eng.* **2015**, *126*, 310–314. [CrossRef]
22. ITTC. ITTC–recommended procedures and guidelines. In Proceedings of the 25th International Towing Tank Conference, Fukuoka, Japan, 14–20 September 2008; ITTC: Fukuoka, Japan, 2008.
23. Liu, D.C.; Hong, F.W. The Numerical Predicted of SMP11 Propeller Performance with and without Cavitation. In Proceedings of the Second International Symposium on Marine Propulsors, SMP'11, Hamburg, Germany, 15–17 June 2011.
24. Chen, K.J.; Wan, D.C. Numerical simulation of cavitation flow in PPTC propeller. In Proceedings of the 29th National Symposium on Hydrodynamics, Zhenjiang, China, 25 August 2018; pp. 632–640.
25. Zhao, M.S.; Wan, D.C. Simulation of propeller cavitation in non-uniform flow field. *China Shipbuild.* **2020**, *61*, 247–253.
26. Feng, X.M.; Cheng, F.M.; Cai, R.Q. Calculation of propeller open water performance by CFD software FLUENT. *Ship Boat* **2006**, *1*, 14–19.

Disclaimer/Publisher's Note: The statements, opinions and data contained in all publications are solely those of the individual author(s) and contributor(s) and not of MDPI and/or the editor(s). MDPI and/or the editor(s) disclaim responsibility for any injury to people or property resulting from any ideas, methods, instructions or products referred to in the content.